3. Yu. A. Buevich, P. L. Mityakin, S. Yu. Pliner, and O. M. Rozental', Inzh.-fiz. Zh., 58, No. 4, 591-596 (1990).
4. Yu. A. Buevich and V. G. Markov, Inzh.-fiz. Zh., 34, No. 6, 1007-1013 (1978).
5. H. Bateman and A. Erdelyi, Tables of Integral Transforms [Russian translation], Vol. 1, Moscow (1969).
6. M. A. Lavrent'ev, Iskusstv. Sputniki Zemli, No. 3, 61-65, Moscow (1959).

MASS-TRANSFER MECHANISM IN A VIBRATIONALLY FLUIDIZED CHEMICAL REACTION DISPERSION

A. F. Ryzhkov, I. E. Kipnis, and A. P. Baskakov

UDC 66.096.5

An elementary analysis is applied to the mass transport mechanism in a solid-state chemical process occurring in a vibrating finely divided mixture. The analysis is confirmed by experiment.

It is usual to conduct a solid-state process involving high-temperature chemical or physicochemical transformations in a material ground to a size level of 0.1-10 μm by means of alternating heating and grinding stages until a single-phase product is obtained. A vibrofluidized bed enables one to combine these stages [1], a key aspect being overcoming sintering, where the solution enables one to optimize the outer interactions.

1. Autohesion Particle Interaction in a High-Temperature Fluidized Bed. The charge usually belongs to group C in Geldart's classification (aspheric particles less than 20-30 μm not fluidized by gas), which coalesce into primary formations under molecular forces. In a stationary bed of chemically inert particles, one gets branched chain structures, which serve to maintain the porosity of $\varepsilon \sim 0.85$-0.95 in a stable state. When the bed is vibrated, the chains are broken and the extreme particles come together to form denser aggregates, whose size in the vibrational-force field may be described by [2]

$$D = \frac{\sigma}{\rho(1-\varepsilon)(1+K_V)g}. \quad (1)$$

That situation occurs for relative small other external forces, including hydrodynamic ones, e.g., in the vibrational treatment of powders in the mobile* state or under low vacuum ($P_0 \leq 10^4$ Pa), when the gas pressure pulsations are at a level close to $P \leq 1$ kPa [4].

Hydrodynamic forces have more effect on the size, as they occur during vibration and are external in relation to the bed. The microporous body has an unsymmetrical force characteristic, and an aggregate has a high hydrodynamic resistance and effectively damps the external gas-pressure pulsations. A positive pulsation compresses the body slightly. A negative pulsation generates tensile forces, which lead to breakup if the tensile strength is exceeded. The pressure-perturbation penetration depth is given by [5], which in our symbols is

$$H_f = \sqrt{a_0^2 \tau_v / \pi f}. \quad (2)$$

The theory shows that the gas pressure amplitude in that range is reduced by a factor e in the pores. Very high tensile forces develop along the channels, with the maximum occurring in the surfaces of the aggregates. One linearizes the pressure distribution to determine the equilibrium diameter of the particle aggregates detached from the initial body by those forces from the proportion

*Classification of vibrational fluidization mode from [3].

Kirov Urals Polytechnical Institute, Sverdlovsk. Translated from Inzhenerno-fizicheskii Zhurnal, No. 2, pp. 209-217, February, 1991. Original article submitted February 12, 1990.

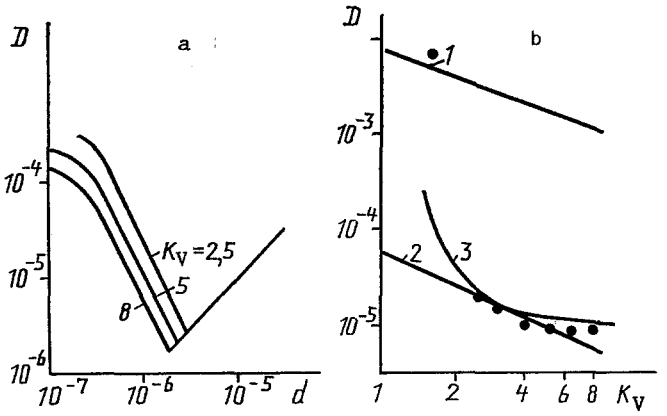

Fig. 1. Aggregate diameter D in a vibrofluidized bed as a function of initial particle size d (a) and of the vibrational acceleration K_V (b): a) from (3) with the [4] data on σ for Al_2O_3 by iteration; b) σ = 0.1 kPa: 1) from (1); 2) from (3) with the [5] formulas; 3) from (3) with the observed dependence of P on K_V [5]; points mean particle size in the final product from the (5) reaction, calculation from [7]; D and d in m.

$$\frac{\sigma}{D} = \frac{P}{2{,}72H_f}. \qquad (3)$$

Here P is half the range in the pressure pulsations in the gas, which varies over the height of the apparatus and in time and which is calculated from the [5] formulas. We substitute for σ from [4] into (3) to get the sizes of the aggregate elements in relation to the initial particle diameter (Fig. 1a). Aggregates migrating through the apparatus are always under nonequilibrium conditions, in which their diameters do not correspond to the gas pressure pulsation level in the given part of the bed. The periodicity of the circulation (about 10^{-1} sec^{-1}) applies to their alternating coalescence and hydrodynamic breakup. This enables one to maintain and renew particle contacts with the retention of the grain-size composition during the vibrational treatment.

Temperature rise increases the autohesion forces to σ of about 0.1-1.0 kPa or more [4], and if there are no gas pressure pulsations (thin bed, mobile condition), the aggregate diameter calculated from (1) approximates to the size of the apparatus, which is equivalent to the bed sintering (Fig. 1b).

When there are gas pressure pulsations (suspended or fountain mode), the size given by (3) approximates to that of the initial particles, which is indirectly confirmed by an experiment in which a charge with d ≈ 2 μm was used that sintered on heating. As the vibrational acceleration increased, the grain-size composition was controlled initially as in (1), and then as in (3) as the gas pressure pulsations developed.

2. Mass Transport Mechanism on Solid-State Interaction. The mechanism in simplified form is considered as existing in two stages for two contacting particles A and B: the material from A covers the surface of B and substance A penetrates into B by diffusion. The supply of A to the surface of B in a stationary bed is provided by prolonged sintering, as in a one-component dispersion, where it is required for Frenkel merging between two solid particles [6]. In a chemically interacting mixture, the coverage is accelerated considerably by the fluctuating contact heat production and the local formation of a mobile phase from substance A, which diffuses over B. Also, substance A may sublime onto the B particles [7]. There is no essential need for sintering here.

The characteristic relaxation times are negligible (10^{-15}-10^{-5} sec [6-8]) for the chemical, diffusion, capillary, and thermal processes by comparison with the periodicity of the forced motion (t_f about 0.02-0.05 sec) and particularly relative to the circulation motion, so one assumes that if the temperature provides for component activity in the contact zone, a solid contact bridge can be formed in a time of about $\Delta t \sim 10^{-3}\ t_f$. The strengths of the crystallization contacts produced under nonequilibrium temperature conditions may be greater by several orders of magnitude than the strengths of the bonds between particles of the same composition [7]. When an aggregate migrates, hydrodynamic disruption occurs

primarily in the unreacted homogeneous parts, which leads to continuous renewal of the reaction surfaces for subsequent contact reaction with the other component and leads to the kinetic stage being maintained until the surfaces of the particles have been completely used up, while the solid state is maintained.

The coverage thus involves several stages:

1) random approach between the different particles during the vibrational mixing;

2) local contact, with gaps less than the molecular-force radius (about 10^{-10} m);

3) chemical and physicochemical transformations at the contacting surfaces;

4) disruption in the resulting crystallization contacts and changes in particle orientation with a frequency of the order of f, which accompanies the reactions in stage 3; and

5) changes in particle aggregation on low-frequency (about 0.1 sec^{-1}) vibrational mixing and the formation of new reaction pairs.

Vibration affects all the stages directly, beginning with accelerating the external diffusion and the renewal of the reaction contacts and ending with the thermal disequilibrium in the diffusion at the surfaces.

The unreacted particle cores interact with the other component via the layer of product by the usual diffusion mechanism, so the reaction time is dependent as usual on the size of the largest fraction and increases in proportion to the square of the aggregate diameter.

Many solid-state processes involve a gas phase [7, 9], the result of which is that the covering rate is higher than the calculated [7] value.

The slip depth s characterizes the mass transfer in a vibrationally fluidized bed, being the distance through which an imaginary point in the gas is displaced along a curvilinear path relative to the particles during an oscillation half-period. The [5] calculated s is about 10^{-6} m ($s/d \approx 1$), so rapid infiltration (proportional to $2\pi f$) involves gas transport from particle to particle into the aggregates or from the free surface into the core of the layer over distances of the order of the grain size d, which is less by three orders of magnitude than the pressure-wave penetration depth Hf. Therefore, the proportion of pores in the aggregates in which the gas is linked up with the flows between them is negligible, and heterogeneous gas–solid interactions occur mainly at the surfaces of the porous aggregates. Within an aggregate, the reactions occur almost as above in the presence of direct contacts between the different types of particles. The mass transfer through the gas in the layer is determined by the particle displacement rate, and the mechanism of interaction through the intermediate gas differs formally very little from the inherent solid-phase reaction.

Identical reaction rates v_{po} and v_p occur in the immobile bed and fluidized one in the external diffusion stage, so one can make simple estimates of how the vibration affects the temperature. The Arrhenius law $v_{p0} = C \exp(-E_a/RT)$ is used with the fact that the reaction rate in the fluidized bed is increased relative to the stationary state in proportion to the likely number of chemical contacts in unit time $n(v_p = v_{p0}n)$, so the reaction temperature in the fluidized bed is

$$T^* = T_0^* - \frac{T_0^* \ln(n)}{E_a/RT_0^* + \ln(n)} . \qquad (4)$$

3. Results and Discussion. These arguments were tested on several reactions. The apparatus included a metal retort 100 mm in diameter made of 12Kh18N10T steel, whose working space was in a shaft oven. The vibrations were communicated to the retort from the core in a VEDS-400 A vibrational tester via a frame linking the two. The retort contained the charge and was closed with a lid having a sampling hole and threaded fitting, which was closed by a hood with insert, and where the components were also cooled by tubes supplying and taking away the gases (or used to evacuate the space), which were connected by flexible rubber tubes to a cylinder containing inert gas and a vacuum pump or trap. When the reactions were conducted in an inert medium, the retort was evacuated and then filled with inert gas. The operation was repeated several times. When samples were taken, inert gas was supplied again, which prevented air from entering. The samples were analyzed for grain size by means of a Fritch Analisette 20 sedimentograph, and also by microscopic examination and XRD, which provided for quantitative analysis [10] with a DRON-2 diffractometer.

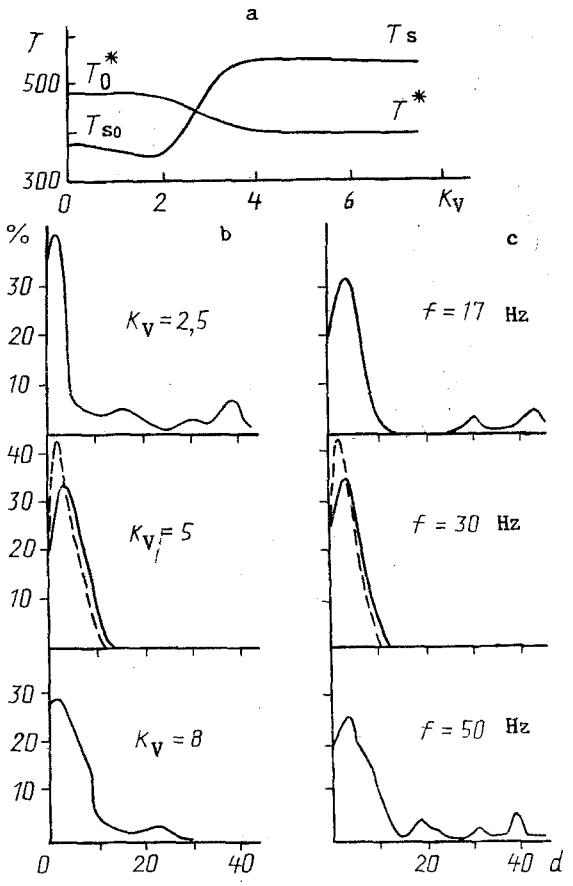

Fig. 2. Sintering temperature T_S (°C) and (5) reaction temperature T* (°C) along with grain-size composition in product with various accelerations (a and b) and vibrational frequencies (c) in the resonant state: a and b) 20 Hz; c) $K_V = 5$; b and c) T = 420°C. The dashed line is the grain-size composition for the initial mixture. T in °C and d in μm.

When gas was produced, a caustic potash solution was used to absorb carbon dioxide. To avoid excess carbon dioxide breaking through, the gas bubbling through a trap containing the solution was trapped by connecting the trap space to a flexible rubber chamber, which expanded when the pressure rose in the trap and contracted as the KOH solution absorbed the carbon dioxide.

We examined the reaction between copper powder and vanadium pentoxide in argon:

$$\underset{\text{orange}}{V_2O_5} + 0{,}6\underset{\text{pink}}{Cu} \rightarrow \underset{\text{black}}{Cu_{0,6}V_2O_5}. \qquad (5)$$

The mass transfer between the copper and V_2O_5 is indicated by the phase diagram [11] as occurring in this temperature range mainly via direct contacts.

We examined how the temperature and vibrational acceleration affected the sintering (Fig. 2a). The copper particles began to sinter long before the reaction began ($T_0^* \approx 480$°C), so for Cu:V_2O_5 (0.6:1) the sintering temperature $T_S = 380$°C in the stationary bed. Vibration to the mobile state, where collisional and inertial forces predominate, caused the sintering to occur for the copper particles at 350°C. The circulation forces in the state tend to break up the sinter into agglomerates, which may be dynamically consolidated and worn in repeated passage along closed circular paths, as occurs in an ordinary vibrational granulator. The particles of the second component, which is inert at this temperature, are also incorporated into the granules. In the suspended state ($K_V = 5$) the reaction temperature T* fell to 400°C (the charge blackened), while the sintering temperature T_S rose to 550°C, so no sintering occurred during the reaction.

To provide a clearer distinction between the chemical and diffusion kinetic zones, the temperature used in the subsequent measurements (T = 420°C), was close to the lower

limit for the reaction. At that temperature, both components were in the solid state.

In the second series of experiments, we determined how the vibration amplitude at the resonant frequency as calculated from [5] affected the product grain size. At low accelerations (K_V < 2.5), the mixture on heating to T > 350°C sintered into a porous agglomerate, in which there was no scope for relative particle displacement. The final product was not a single-phase one.

At T > T_V (450-500°C), the sinter obtained with K_V = 2.5 rapidly strengthened, and on stronger vibration (K_V = 5-8) began to shift about in the reactor, where it behaved as a rigid porous body and gave a characteristic metallic sound on collision with the bottom.

With more vigorous vibration (K_V = 2.5-3), the particles remained mobile in the bed throughout the treatment. After cooling, the mixture consisted of about 70% of reacted powder with enlarged grains, but still similar to the initial material, and to about 30% of newly formed 10-40 μm particles (Fig. 2b). The microscope showed that the latter consisted of sinters of the initial components cemented together by crystalline products.

The Fig. 3a kinetic curves indicate that there are differences in reaction rate even for K_V = 3 in the initial period (kinetic range I), which are related to accelerated mixing, but they vanish in the diffusion-limited region II, and the process dies away as in an immobile bed. This conflicts with the Ginstling–Braunstein model used in describing such reactions [11] (Fig. 3a, dashed lines) and corresponds more closely to current views on mass transfer in granular systems containing interacting phases [12]. The grain-size composition and the packing between the different types of particle vary during the vibrational treatment only slightly in that state.

In the suspended state with small-scale fountaining (K_V = 5), the sinters vanish and the product grain-size composition is similar to the initial one, while the process goes to completion much more quickly (Fig. 4a).

On large-scale low-frequency fountaining (K_V = 8), the particles spend part of their time in the deposited layer (dense or mobile) or as ejector in the space above the bed, which leads to a smaller extent to sinters that retard the reaction. Another source of sinters is provided by the wall deposits formed on fountaining in the upper parts of the retort.

As the resonant frequency is varied with K_V = idem, the pattern is reproduced (Fig. 2c). At low frequencies, which cause large-scale fountaining, and also at high frequencies, which do not produce appreciable bed expansion, one gets the above aggregates of 30-40 μm size, and the content of the main substance in the final product is reduced (Fig. 4b). The reaction time calculated from the Ginstling–Braunstein equation agrees well with observation within the range of vibration parameters providing a homogeneous grain-size composition (K_V = 5-7, f = 20-30 Hz) and reduces the homogenization time at which sinters occur.

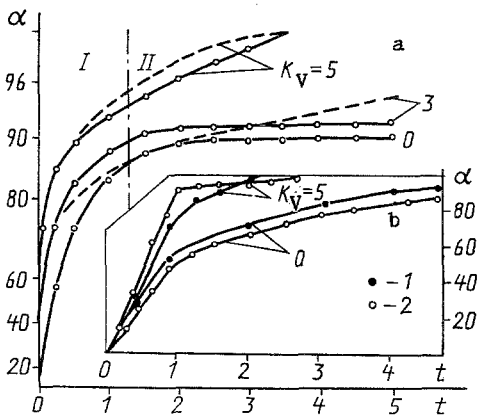

Fig. 3. Kinetic curves for the degree of conversion α and time t in the resonant state in vibrational fluidization: a) reaction (5), T=420°C, f=20 Hz. Dashed lines derived from the Ginstling–Braunstein equation [9] by the [7] method; b) reaction occurring via the gas: 1) reaction (6), T = 700°C, f = 20 Hz; 2) (7), T = 750°C, f = 20 Hz, α in % and t in h.

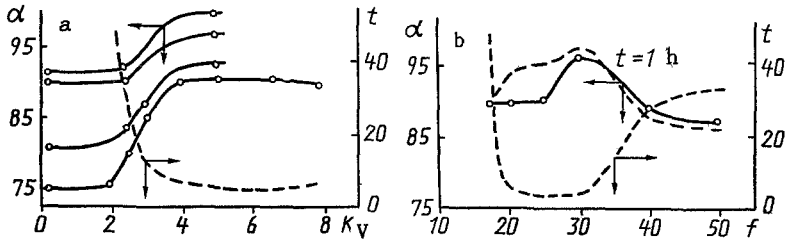

Fig. 4. Dependence of degree of conversion α and homogenization time t in (5) on acceleration (a) and frequency (b) in the resonant state: a) 20 Hz; b) K_V = 5; points from XRD; T = 420°C; dashed curves from the Ginstling–Braunstein equation for the actual composition, and t time corresponding to α = 99.95%.

Interactions involving the gas were examined on the basis of the reaction between copper oxide and copper powder:

$$CuO + Cu \rightarrow Cu_2O. \quad (6)$$

The copper–oxygen phase diagram [13] indicates that two equilibria occur at 375-900°C:

$$4CuO_{(s)} = 2Cu_2O_{(s)} + O_{2(g)}, \quad (6a)$$

$$2Cu_2O_{(s)} = 4Cu_{(sss)} + O_{2(g)}. \quad (6b)$$

Above 700°C, copper oxide is [11] absolutely unstable and dissociates almost entirely with oxygen release. In suspended vibrational fluidization, there are copper particles nearby at distances of the order of s, which are oxidized to cuprous oxide, so the reaction goes to completion (Fig. 3b). In a stationary layer, the charge sinters at 400°C, which hinders the oxygen diffusion within the enlarged sinters and the reaction dies away.

The vibrational fluidization affects the chain reactions between the solids occurring via the intermediate gas phase [9], as for example in the reactions of metal oxides with carbon. The intensive mixing of the solid and intermediate gas components in the carbothermal reduction of cobalt oxides in a vibrationally fluidized bed enables one to avoid local depletion in the reducing agent and ensures that the reaction goes to completion (Fig. 3b):

$$Co_3O_4 + \frac{1}{2}C \rightarrow 3CoO + \frac{1}{2}CO_2, \quad (7)$$

which according to [14] combines the dissociation of Co_3O_4 with the gasification of the carbon and the reduction of the residual Co_3O_4 by carbon monoxide.

The measured temperatures in (6) and (7) agree well with calculations from (4) (Table 1). The n estimated in the calculations from elementary considerations is about 3-20, while the E_a for the calculations were taken from [9].

Notation. A) vibration amplitude; a_0) equilibrium speed of sound in the dispersed medium; c) preexponential factor in the Arrhenius equation; d) particle diameter; D) aggregate diameter; E_a) activation energy; f) vibrational frequency; g) acceleration due to

TABLE 1. Minimal Temperatures for the Completion of Reactions (6) and (7) in an Immobile Bed and on Vibrational Fluidization

Reaction number in text	Rate-limiting step	E_a, kJ/mole	ln(n)	calc. °C	Measured, °C	
				$\Delta T = T_0^* - T^*$	T_0^*	T^*
6	$2CuO \rightarrow Cu_2O + O$	56	1—3	85—210	800	650
7	$Co_3O_4 \rightarrow 3CoO + O$	356	1—3	17—48	800	750

gravity; H) bed depth; H_f) pressure wave penetration depth; K_v) relative vibrational acceleration; n) likely number of chemical contacts for a particle during vibrational mixing; P_0) environmental pressure; P) half-range for gas pressure pulsations in bed; R) universal gas constant; s) phase slip depth [5]; T) temperature; t) time; t_v) vibration period; v_p) reaction rate; ε) porosity; ρ) particle density; σ) autohesion bond strength; τ_v) phase velocity relaxation time [5]; α) degree of conversion.

LITERATURE CITED

1. A. P. Baskakov, I. E. Kipnis, A. F. Ryzhkov, et al., "Development prospects for fluidization techniques," Abstracts for an All-Union Conference [in Russian], Leningrad (1988), pp. 17-18.
2. Ya. M. Shchelokov, A. M. Avvakumov, and Yu. K. Sazylin, Cleaning Heating Surfaces in Utilizer Boilers [in Russian], Moscow (1984).
3. A. P. Baskakov (ed.), Heat and Mass Transfer in Fluidized Beds [in Russian], Moscow (1978).
4. A. D. Zimon and E. I. Andrianov, Powder-Material Autohesion [in Russian], Moscow (1978).
5. A. F. Ryzhkov and B. A. Putrik, Inzh.-fiz. Zh., 54, No. 2, 188-197 (1988).
6. Ya. B. Geguzin, Sintering Physics [in Russian], Moscow (1984).
7. P. P. Budnikov and A. M. Ginstling, Reactions in Mixtures of Solids [in Russian], Moscow (1971).
8. G. A. Abduragimov, R. P. Meilanov, and Ya. L. Ugai, Inzh.-fiz. Zh., 50, No. 6, 1013-1017 (1986).
9. M. Brown, D. Dollimore, and A. Galway, The Reactions of Solids [Russian translation], Moscow (1983).
10. L. M. Kovba and V. K. Trunov, X-ray Phase Analysis [in Russian], Moscow (1976).
11. A. A. Fotiev, V. L. Volkov, and V. K. Kapustkin, Vanadium Oxide Bronzes [in Russian], Moscow (1978).
12. P. M. Vaisblat and S. L. Komarinskii, Heat and Mass Transfer: International Conference Abstracts, Section 5, Heat and Mass Transfer in Dispersed Systems [in Russian], Minsk (1988), pp. 13-15.
13. O. A. Esin and P. V. Gel'd, The Physical Chemistry of Pyrometallurgical Processes [in Russian], Sverdlovsk (1962).
14. A. K. Ashin and S. T. Rostovtsev, Izv. Vyssh. Uchebn. Zaved., Chernaya Metallurgiya, No. 11, 5-9 (1967).

HEAT TRANSFER AND COMBUSTION FOR A SPIRAL FLOW IN AN IDEAL-DISPLACEMENT REACTOR

I. G. Dik and O. V. Matvienko

UDC 532.542.2:536.25.27:536.46

Hydrodynamic equations have been used with a numerical method to construct the temperature and concentration patterns for a reacting gas. Heat transfer in an ideal-displacement reactor is examined along with the structure of the reaction zone for various values of the spiral flow parameters.

Formulation. Heat transfer, reaction, and ignition in internal flows have various applications [1-6].

The temperature patterns in a reacting flow is related to a considerable extent to the marked temperature dependence of the rate, which governs the flame propagation rate (reaction zone) if the reaction is highly exothermic. Under stationary conditions, the reaction zone propagates upstream as a combustion front. The front is stabilized at a certain distance from the reagent input, at a point dependent on the relation between the input

Kuibyshev Tomsk University.

Translated from Inzhenerno-fizicheskii Zhurnal, No. 2, pp. 217-225, February, 1991. Original article submitted December 4, 1989.